J Ther Eng, Vol. 8, No. 1, pp. 78–89, January 2022

Journal of Thermal Engineering
Web page info: https://jten.yildiz.edu.tr
DOI: 10.14744/jten.2022.xxxx

Journal of Thermal Engineering

Research Article

Parametric optimization of blowdown operated double-effect vapour absorption refrigeration system

Deshdeep GAMBHIR[1], Ahmad Faizan SHERWANI[1], Akhilesh ARORA[2], Ashwni[1,*]

[1]Department of Mechanical Engineering, Jamia Millia Islamia, Jamia Nagar, New Delhi, Delhi 110025, India
[2]Department of Mechanical Engineering, Delhi Technological University, New Delhi-110 042, India

ARTICLE INFO

Article history
Received: 13 February 2021
Accepted: 27 May 2021

Keywords:
Double-effect vapour absorption refrigeration system; Exergy; Cogeneration; RSM; ANOVA

ABSTRACT

The present work investigates the thermodynamic optimality of a double-effect vapor absorption refrigeration system (VARS) driven by blowdown heat of a 210 MW thermal power plant at Badarpur using response surface methodology (RSM). RSM helps to develop a relation amongst the decision variables and the second law efficiency via second-order nonlinear polynomial regression equation. In addition, the analysis of variance technique (ANOVA) is applied to identify the decision variables having a significant effect on the system's thermal performance. Moreover, coefficient of structural bond (CSB) analysis of the evaporator is carried out. The decision variables are the temperatures of the high-pressure generator, low-pressure generator, condenser, absorber, and evaporator. Results conclude that the second law efficiency is affected significantly by absorber temperature (F value = 2049.4), followed by condenser temperature (F value = 1596.4), and is least affected by high-pressure generator temperature (F value = 495). CSB value of the Evaporator is 0.5851.

Cite this article as: Deshdeep G, Ahmad F S, Akhilesh A, Ashwni. Parametric optimization of blowdown operated double-effect vapour absorption refrigeration system. J Ther Eng 2022;8(1):78–89.

INTRODUCTION

The combined cooling, heat, and power (CCHP) cycle is used for the production of power, cooling, and heating simultaneously from one primary energy source. The CCHP cycle is advantageous as it limits the use of primary energy which leads to a reduction in load experienced by the power plant. This reduction in the load on the power plant assists the reduction in harmful emissions to the environment and also decreases the fossil fuel requirement. The most significant aspect of the CCHP cycle is that it utilizes renewable forms of energy or waste energy to operate a refrigeration cycle. Renewable forms of energy can be solar, wind, tidal and geothermal while the waste heat sources include exhaust from the gas turbine, gas-steam combined cycle, automotive vehicle, the flue gas of boiler. Even bleed

***Corresponding author.**
*E-mail address: ashwanigoyal617@gmail.com

This paper was recommended for publication in revised form by Regional Editor Jaap Hoffman Hoffman

Published by Yıldız Technical University Press, İstanbul, Turkey

steam of steam turbines, as well as the heat of blowdown operation, can be used to provide the necessary energy required by the generator of VARS.

The multiple benefits of the CCHP cycle made researchers conduct studies to improve its thermodynamic performance. Abed et al. [1] conducted a parametric study to investigate the effect of input variables on the thermodynamic functioning of combined Rankine and absorption refrigeration cycle with propane-decane as the organic dual working fluid through the development of mathematical mode. Fontalvo et al. [2] investigated total exergy destruction and studied the input factors such as ammonia mass fraction and pressure ratio along with their effects. These were studied in terms of absorber and turbine efficiency. An analysis was also carried out to study the influence of internal and external cooling for rectification. Rego et al. [3] experimentally investigated the absorption refrigeration system which was powered by the heat rejected from the automotive vehicles i.e. exhaust heat. Parvez and Khaliq [4] analyzed the second law analysis of the biomass-fuelled cogeneration cycle and found the combustion chamber accountable for 25% exergy destruction. Goyal et al. [5] modified a diesel engine having a single-cylinder of 3.7 kW capacity into a cogeneration system to study the generation of power and cooling process. Yang et al. [6] analyzed the exergy destruction at the ejector in a combined power and ejector refrigeration cycle, concluding it to be more than 40%. Singh [7] conducted a second law analysis of the combined Brayton- Rankine power cycle integrated with the ammonia-water VARS. Talukdar and Gogoi [8] conducted an exergetic analysis of the LiBr-H_2O VARS where waste heat from boiler flue gas became the source of heat and concluded a reduction in total exergy destruction when the temperature of the high-pressure generator was increased. Jain et al. [9] used advanced exergy analysis to identify the components on which efforts can be applied to reduce their exergy destructions.

In most cases, the objective of the CCHP cycle is space cooling, process heating, and power production from the same primary energy but some researchers felt the need of reducing condenser load by this cycle. Ifaei et al. [10] used bleed steam of steam turbine as a source of heat to run a single-effect vapor absorption refrigeration cycle. The salient feature of this work is that although there is a slight decrease in the thermal efficiency of the steam cycle yet it was compensated by the reduced requirement of the makeup water in the cooling tower. So, such a cycle could be used where water is scarce. One of the major limitations of using waste heat to run the refrigeration cycle is that it fouls the heat exchanger, which leads to a decrease in its effectiveness over a period. The solution to this problem is to utilize a renewable form of energy to run the refrigeration cycle. The most commonly used renewable form of energy is solar energy and geothermal energy. Guo et al. [11] worked on the geothermal source with the cycle of vapor absorption. The principal aim of this research includes the determination of appropriate working fluid and further optimization of cycle variables.

The above-mentioned research works are related to the first law analysis, the second law analysis, and the multi-objective optimization of the system. However, the above-mentioned analyses lack in determining the most influencing decision variables, which affect the performance of the system. Response surface methodology (RSM) is such a statistical optimization technique that can be used to determine the most influencing decision variables. It is a set of mathematical and statistical techniques that can be used to define the effect of independent variables, alone or in combination, on the output by generating a mathematical model. Goyal et al. [12] in their research paper studied the effect of source temperature, sink temperature, mass fraction, isentropic efficiency of the turbine, isentropic efficiency of the pump, and effectiveness of internal heat exchanger (IHE) on the thermal efficiency of organic Rankine cycle by using RSM technique. RSM has many advantages but still, very little work has been done on the CCHP cycle.

In the present paper, a series flow double-effect vapor absorption refrigeration system (VARS) run by the waste heat of blowdown operation is thermodynamically analyzed and optimized with the help of RSM to identify the most significant decision variables based on its thermal performance. The second law efficiency is taken as the performance parameter and decision variables are absorber temperature, condenser temperature, evaporator temperature, the temperature of the high-pressure generator, and temperature of the low-pressure generator. Moreover, the CSB analysis of the evaporator is done to determine its sensitivity.

DESCRIPTION OF THE SYSTEM

Figure 1 shows the schematic diagram of the proposed double-effect VARS. The weak solution of Li-Br coming out of the absorber (state 4) is pressurized by pump up to high-pressure generator (HPG) Pressure (state 5). Then it passes through solution heat exchanger 1 to recovers heat from the strong Li-Br solution coming out of a low-pressure generator (LPG). This solution then enters (state 6) solution heat exchanger 2 where its temperature is further raised. At state 7, it passes through HPG where external heat is supplied by a steam drum consisting of blowdown water (state 18 to state 19). In HPG, at state 11 the solution splits into refrigerant 1 (water vapor) which passes through LPG, and a strong Li-Br mixture at state 8. LPG recovers the heat from the refrigerant by behaving as an internal heat exchanger to further generate at state 14, the refrigerant 2, and a strong Li-Br mixture. Heat is exchanged at state 9 when the Li-Br mixture from HPG (state 8) passes through solution heat exchanger 2. Further, this mixture flows from the pressure

reducing valve 2 (state 9 to state 10), the LPG (state 15) to solution heat exchanger 1 for the process of heat exchange (state 16). The pressure is reduced to condenser pressure (state 13) when refrigerant 1 after exiting the LPG (state 12) passes through the pressure reducing valve 3. Refrigerant 2 and refrigerant 1 mix in the condenser and the mixed refrigerant is externally cooled by water (state 20 to state 21). Then, it is throttled up to evaporator pressure (state 1 to state 2) and evaporates in the evaporator by cooling external water (state 22 to state 23). At the exit of the evaporator, while passing through the absorber, the mixed refrigerant combines with the strong Li-Br mixture, which is returning from solution heat exchanger 1 through reducing valve 1 (state 16 to state 17). The absorber is externlly cooled by water to dissipate the heat of absorption (state 24 to state 25). This cycle then repeats.

THERMODYNAMIC MODELLING

Few assumptions have been considered for the thermodynamic modelling of the proposed system which are listed below [13]:

- Steady-state operating condition.
- The concentration of the LiBr-H_2O solution is at equilibrium at the respective temperature and pressure.
- There is no loss of pressure in the heat exchangers and the connecting piping.
- Li-Br solution concentration remains the same when the heat is transferred to the solution heat exchanger.
- There are no losses of heat transfer occurring between connecting pipes and the environment.
- The state of water is saturated vapor at the exit of the evaporator and is saturated liquid at the exit of the condenser.

PROCEDURE FOR MODELLING A DOUBLE EFFECT REFRIGERATION SYSTEM

- Input values of temperatures at cooling load, evaporator, condenser, high-pressure generator, low-pressure generator, blowdown water inlet and outlet, the effectiveness of solution heat Exchangers 1 and 2, and mass of blowdown water available [Table 1] are fed to the system.

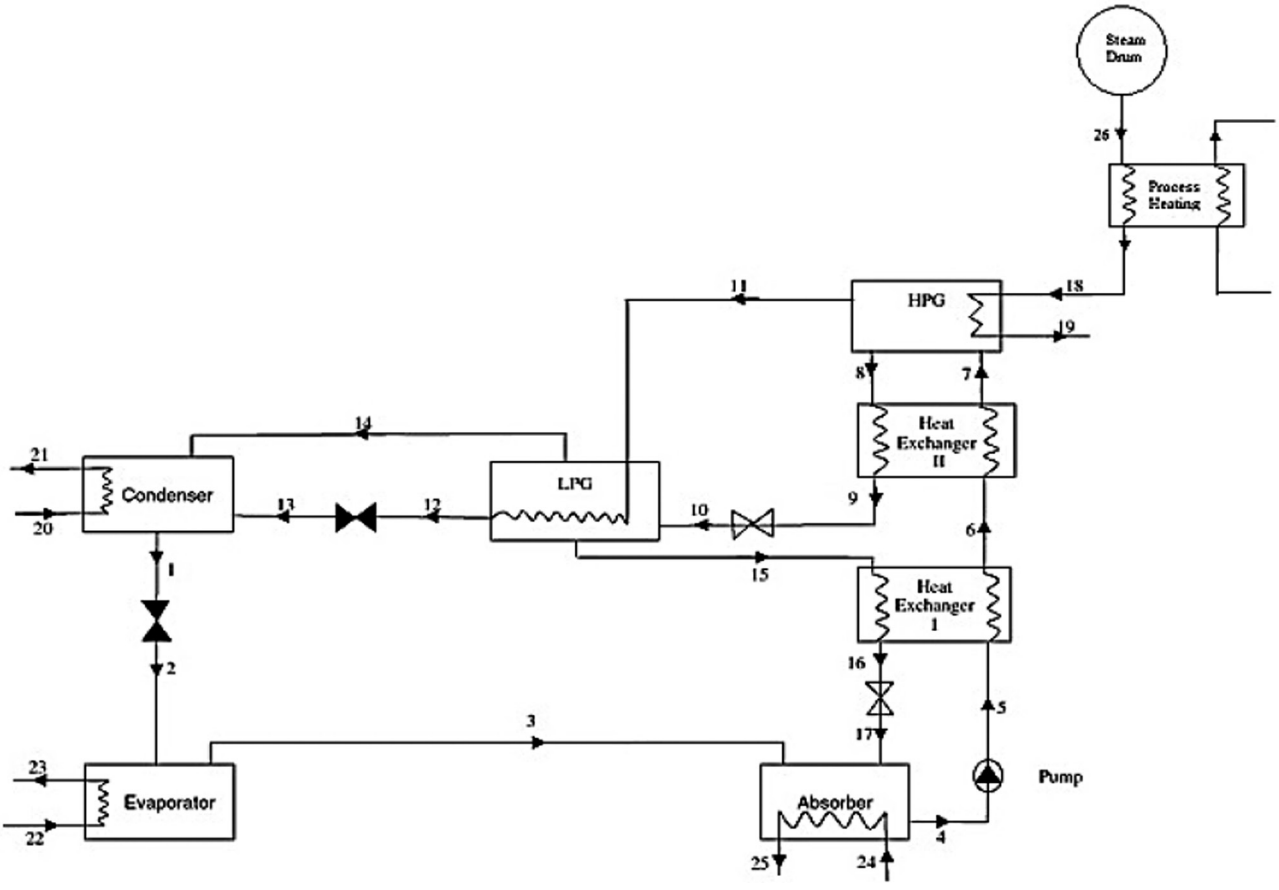

Figure 1. Schematic diagram of a double-effect vapor absorption refrigeration system.

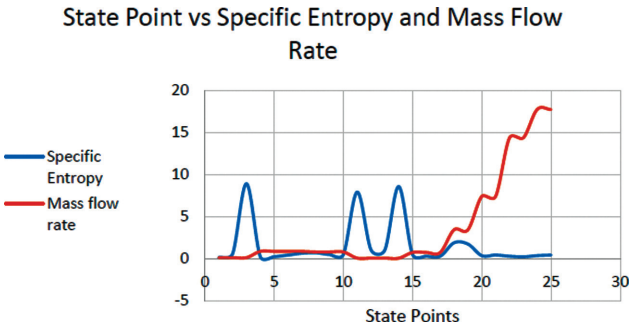

Figure 2. State points vs specific entropy and mass flow rate.

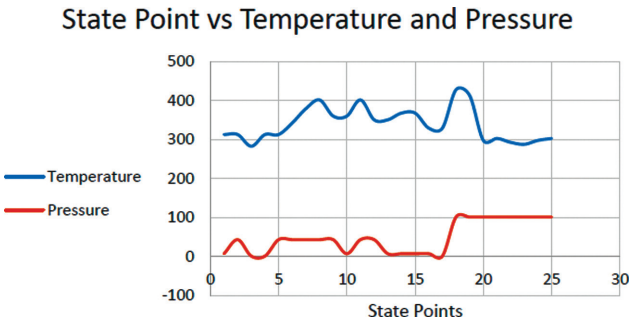

Figure 3. State points vs temperature and pressure.

Table 1. Data used as input for simulation

Sr. No.	Description (Abbreviation)	Value(s)
1	Ambient temperature (T_o)	25°C
2	Condenser temperature (T_1)	40°C
3	Evaporator temperature (T_3)	10°C
4	Absorber temperature (T_4)	40°C
5	High-pressure generator temperature (T_8)	148.9°C
6	Low-pressure generator temperature (T_{15})	95°C
7	Blowdown inlet water temperature (T_{18})	155°C
8	Blowdown outlet water temperature (T_{19})	140°C
9	Cooling water inlet temperature to condenser (T_{20})	25°C
10	Cooling water outlet temperature from the condenser (T_{21})	30°C
11	Water inlet temperature to the evaporator (T_{22})	15°C
12	Water outlet temperature from the evaporator (T_{23})	20°C
13	Cooling water inlet temperature to the absorber (T_{24})	25°C
14	Cooling water inlet temperature from the absorber (T_{25})	30°C
15	Cooling load (Q_e)	300 KW
16	Effectiveness of solution heat exchanger 1 (ε_1)	0.7
17	Effectiveness of solution heat exchanger 2 (ε_2)	0.7
18	Pump isentropic efficiency (η)	0.95

- The temperature values at the inlet and outlet of external fluid of condenser, absorber, and evaporator, are also fed [Table 1].
- Determine the properties of refrigerant and solution at relevant state points using engineering equation solver (EES) software (refer to Figures 2,3 and 4) [14].
- Apply conservation equations for mass and concentration, and energy balance equation [15] to determine mass flow rate, the concentration of refrigerant as well as of solution, and the heat transfer for high-pressure generator, low-pressure generator, condenser, and absorber [Table 2].
- Calculate the irreversibility for the complete system and also for individual components. Finally, compute the second law efficiency of VARS [Table 3].

OPTIMIZATION METHODOLOGY

We have utilized the principle of steepest ascent-based Response Surface Methodology (RSM) for the parametric optimization [12]. By modelling the often-complex relationship that may exist between a multitude of input variables (X_1, X_2, … … ., X_n) and their corresponding response/decision-variable, Y, the RSM technique utilizes

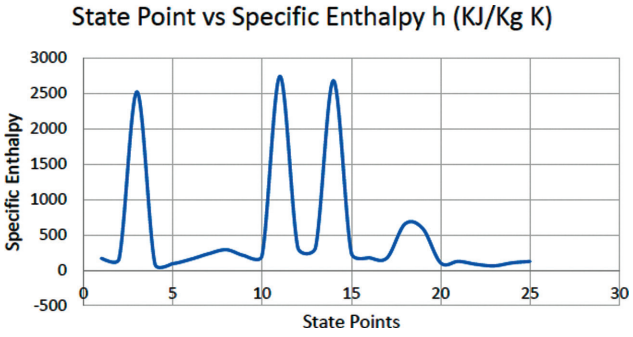

Figure 4. State points vs specific enthalpy.

a combined mathematical-statistical approach to efficiently compute the optimal values for the input variables. As such, the generic equation describing the mathematical model between the input and output variables is expressed using Equation (1):

$$Y = f(X_1, X_2, \ldots\ldots, X_n + \varepsilon_{er}) \quad (1)$$

Where f is output response and $\boldsymbol{\varepsilon}_{er}$ is the error computed when the model is computed. The corresponding 2nd-order regression model is described by Equation (2) [12] and shown below.

Table 2. Equations dependent on mass, energy, and concentration conservation

Components	Equations based on conservation of mass, concentration, and energy
Absorber	$m_1 + m_{15} = m_4$ $m_4 X_4 = m_{15} X_{15}$ $Q_{abs} = m_1 h_3 + m_{15} h_{17} - m_4 h_4$ $C_{pw} = 4.187$ kJ/kg-K $Q_{abs} = m_{24} C_{pw} (T_{25} - T_{24})$
Pump	$\delta P = P_{hpg} - P_{abs}$ $W_p = \frac{m_4 \delta P}{\rho_4 \eta_p}$ $h_5 = h_4 + W_p$
Solution heat exchanger 1	$\varepsilon_1 = \frac{T_{15} - T_{16}}{T_{15} - T_5}$ $\quad m_4 C_5 (T_6 - T_5) = m_{15} C_{15} (T_{15} - T_{16})$
Solution heat exchanger 2	$\varepsilon_2 = \frac{T_8 - T_9}{T_8 - T_6}$ $\quad m_4 C_6 (T_7 - T_6) = m_8 C_8 (T_8 - T_9)$
HPG	$m_8 + m_{11} = m_4$ $Q_{hpg} = m_{11} h_{11} + m_8 h_8 - m_4 h_7$ $Q_{hpg} = m_{18} C_{pw} (T_{18} - T_{19})$
LPG	$m_8 = m_{14} + m_{15}$ $m_8 X_8 = m_{15} X_{15}$ $Q_{lpg} = m_{11} (h_{11} - h_{12}) + m_8 h_{10} - m_{15} h_{15} - m_{14} h_{14}$
Condenser	$m_1 = m_{11} + m_{14}$ $Q_c = m_{14} h_{14} + m_{11} h_{13} - m_1 h_1$ $Q_c = m_{20} C_{pw} (T_{21} - T_{20})$
Evaporator	$m_1 = \frac{Q_e}{(h_3 - h_2)}$ $Q_e = m_{22} C_{pw} (T_{22} - T_{23})$

Table 3. Mathematical expressions based on the second law of analysis

Components	Mathematical Expressions
Absorber	$I_{abs} = T_o\left(\left(m_4 s_4 - m_{15} s_{17} - m_3 s_3\right) + m_{24} C_{pw} \ln\left(\frac{T_{25}}{T_{24}}\right)\right)$
Pump	$I_p = T_o\left(s_5 - s_4\right)$
Solution heat exchanger 1	$I_{shx1} = T_o\left(m_{15} C_{pw} \ln\left(\frac{T_{16}}{T_{15}}\right) + m_4 C_{pw} \ln\left(\frac{T_6}{T_5}\right)\right)$
Solution heat exchanger 2	$I_{shx2} = T_o\left(m_8 C_{pw} \ln\left(\frac{T_9}{T_8}\right) + m_4 C_{pw} \ln\left(\frac{T_7}{T_6}\right)\right)$
HPG	$I_{hpg} = T_o\left(\left(-m_4 s_7 + m_8 s_8 + m_{11} s_{11}\right) + m_{14} C_{pw1} \ln\left(\frac{T_{19}}{T_{18}}\right)\right)$
LPG	$I_{lpg} = T_o\left(m_{15} s_{15} + m_{11} s_{12} - m_{11} s_{11} - m_8 s_{10} + m_{14} s_{14}\right)$
Condenser	$I_{cond} = T_o\left(\left(-m_4 s_{14} - m_{11} s_{13} + m_1 s_1\right) + m_{20} C_{pw} \ln\left(\frac{T_{21}}{T_{20}}\right)\right)$
Evaporator	$I_{evap} = T_o\left(m_1\left(s_3 - s_2\right) + m_{22} C_{pw} \ln\left(\frac{T_{23}}{T_{22}}\right)\right)$
Expansion device	$I_{exp} = T_o\left(m_1 * \left(s_2 - s_1\right)\right)$
Second law efficiency	$= \frac{I_{tot}}{E_{in}}$
	$I_{tot} = I_{abs} + I_{shx1} + I_{shx2} + I_{hpg} + I_{exp} + I_{lpg} + I_{cond} + I_{evap}$
	$E_{in} = \left(1 - \frac{T_o}{T_{avg}}\right) Q_{hpg}$
	$T_{avg} = T_{hpg} + 273$

$$Y = \beta_0 + \sum_{i=1}^{n} \beta_i X_i + \sum_{i=1}^{n} \beta_{ii} X_i^2 + \sum_{i<j}^{n} \beta_{ij} X_i X_j \quad (2)$$

Where β_0, β_i, β_{ii} and β_{ij} are the interception, linear, quadratic and interaction coefficients, respectively.

ORTHOGONAL ARRAY (OA)

In the present work, the second law efficiency is the chosen response variable while high-pressure generator temperature, low-pressure generator temperature, absorber temperature, Condenser temperature, and evaporator temperature are chosen as decision variables. Therefore, there are five decision variables and one response variable. For Five decision variables with three levels, the chosen OA design is L_{27}, given in Table 4 [16,17].

ANALYSIS OF DATA

The data given in Table 5 were analyzed by the RSM module of Minitab 18.1 [18]. This software determines the coefficients of the second-order polynomial Equation (2). Moreover, it provides the contour plots as well as three-dimensional surface plots of the model. In addition to

Table 4. L27 Orthogonal Array

Tc	Tabs	Tlpg	Thpg	Te	Second law efficiency
35	35	90	145	6	0.1803
35	35	90	145	8	0.1847
35	35	90	145	10	0.1889
35	40	95	150	6	0.1683
35	40	95	150	8	0.1722
35	40	95	150	10	0.176
35	45	100	155	6	0.1582
35	45	100	155	8	0.1621
35	45	100	155	10	0.1654
40	35	95	155	6	0.1645
40	35	95	155	8	0.169
40	35	95	155	10	0.1734
40	40	100	145	6	0.1725
40	40	100	145	8	0.1767
40	40	100	145	10	0.1805
40	45	90	150	6	0.1255
40	45	90	150	8	0.1433
40	45	90	150	10	0.1546
45	35	100	150	6	0.1682
45	35	100	150	8	0.1731
45	35	100	150	10	0.1775
45	40	90	155	6	0.1141
45	40	90	155	8	0.1342
45	40	90	155	10	0.1473
45	45	95	145	6	0.1235
45	45	95	145	8	0.1443

RSM, analysis of variance (ANOVA) is used to check the adequacy of the model.

RESULT AND DISCUSSION

Model Validation

The present thermodynamic Model of the proposed system has been validated with the work done by reference [19] under the same input conditions and working fluid. The results of the validation are presented in Table 6.

ANALYSIS AND INTERPRETATION OF THE MODEL

ANOVA, a collection of models and procedures, analyses, and estimates various parameters such as probability plot (nP plot), p-values, F-values, and coefficient of determination to identify the model's suitability. The validity of ANOVA is governed by the normal probability plot which investigates the residuals.

It is worth mentioning that residuals for the response variable of VARS follow a normal distribution. P-values (Table 5) help in identifying the significant effect of decision variables on the output parameters. The effect on the output parameter is said to be significant if the p-value is less than 0.05. These values also estimate the effect of interactions on output variables.

Table 5. Analysis of Variance

Source	DF	F-Value	P-Value	Remarks
Model	14	437.91	0.000	
Linear	5	1150.48	0.000	
Tc	1	1596.44	0.000	
Ta	1	2049.43	0.000	
Tlpg	1	886.15	0.000	
Thpg	1	495.37	0.000	
Te	1	725.02	0.000	
Square	5	5.80	0.006	Non-significant
Tc*Tc	1	6.70	0.024	Non-significant
Ta*Ta	1	10.42	0.007	Non-significant
Tlpg*Tlpg	1	1.11	0.312	Non-significant
Thpg*Thpg	1	4.72	0.050	Non-significant
Te*Te	1	6.06	0.030	Non-significant
2-Way Interaction	4	87.32	0.000	
Tc*Te	1	142.97	0.000	
Ta*Te	1	96.23	0.000	
Tlpg*Te	1	109.99	0.000	
Thpg*Te	1	0.07	0.791	Non-significant
R-sq	99.80%			
R-sq(adj)	99.58%			
R-sq(pred)	99.00%			

Table 6. Model validation

Sr. No	Component	Quantity	Present Work	Reference [19]	Percentage Error
1	Absorber	Qabs	2954	2942.175	0.40
2	Condenser	Qcond	1351	1282.052	5.37
3	HPG	Qhpg	1897	1868.1	1.54
4	COP		1.242	1.26	1.42

The second-order polynomial Equation (2) can be transformed into a mathematical model that is developed through fitting response data and is given in Equation (3). The least-square methodology, a multi-regression technique, helps in generating this mathematical model.

The following terms cannot be estimated and were removed: Tc*Ta, Tc*Tlpg, Tc*Thpg, Ta*Tlpg, Ta*Thpg, Tlpg*Thpg.

Regression Equation (3) in uncoded units is given as follows:

$$\begin{aligned}\text{Second law efficiency} &= 0.504 - 0.00161\ \text{Tc} \\ &- 0.01101\ \text{Ta} + 0.00071\ \text{Tlpg} + 0.01234\ \text{Thpg} \\ &+ 0.01532\ \text{Te} - 0.000054\ \text{Tc}^2 + 0.000067\ \text{Ta}^2 \\ &+ 0.000022\ \text{Tlpg}^2 - 0.000045\ \text{Thpg}^2 - 0.000321\ \text{Te}^2 \\ &+ 0.000441\ \text{TcTe} + 0.000362\ \text{TaTe} - 0.000387\ \text{TlpgTe} \\ &- 0.000010\ \text{ThpgTe}\end{aligned} \tag{3}$$

The significance of the model defined by the above Equation (3) can be determined by F-value which governs its statistical significance along with the decision variables and their interactions. The effect of the decision variable on the output parameter is significant if the F-value is high.

From Table 5 it is noted that the maximum F value is 2049.43 for absorber temperature and the minimum F value is 495.32 for high-pressure generator. It means that the second law of efficiency is mostly affected by absorber temperature and least affected by high-pressure generator temperature. The R^2 value for the present model is 99.8% that again confirms the validity of the results of ANOVA determined above.

GRAPHICAL RESULTS: CONTOUR PLOTS

- Contour plots or response surface plots are graphical 2D representations that show the effect of decision variables on the response variable. The following section highlights the inferences drawn from the contour plots on the second law efficiency.

Contour Plot of Second Law Efficiency vs T_A, T_C

Figure 5 is the contour plot of second law efficiency for decision variable T_c on the X-axis and T_a on the Y-axis. The area under the dark green color in the plot represents the highest second law efficiency value which is more than 0.18 observed at a low value of T_a and T_c. Conversely, the minimum value which is less than 0.14 is achieved at a high condenser and absorber temperature.

Contour Plot of Second Law Efficiency vs T_{LPG}, T_C

Figure 6 is the contour plot of second law efficiency for decision variable T_c on the X-axis and T_{lpg} on the Y-axis. The area under the dark green color represents the maximum second law efficiency i.e. more than 0.18. This maximum efficiency is achieved at low T_c and high T_{lpg}. Conversely, the minimum second law of efficiency is less than 0.15 and is achieved at a high condenser temperature and low temperature of LPG. The significance of this contour plot is that condenser temperature depends upon environmental conditions so, in summer i.e. higher T_c, the value of second law efficiency can be maintained by raising the low-pressure generator temperature.

Contour Plot of Second Law Efficiency vs T_{HPG}, T_C

Figure 7 is the contour plot of second law efficiency for decision variables T_c and T_{hpg} on the X-axis and Y-axis respectively. The maximum value is more than 0.175, which

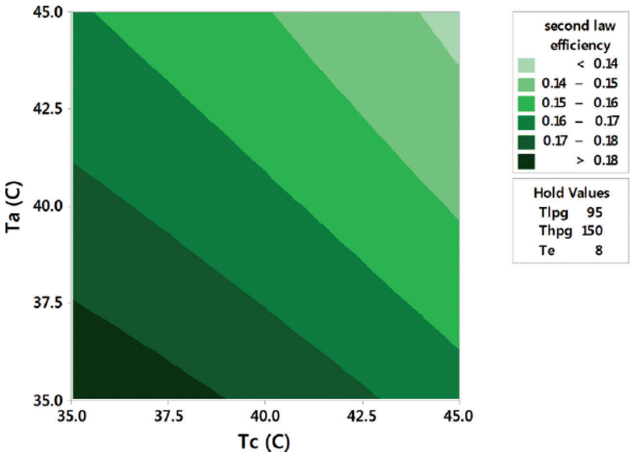

Figure 5. Contour plot of second law efficiency vs T_a, T_c.

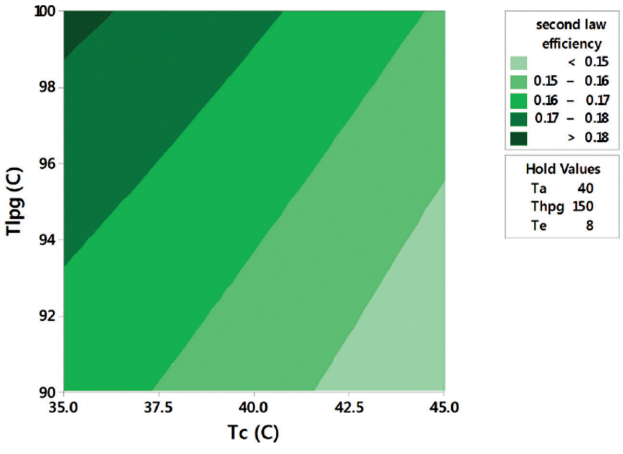

Figure 6. Contour plot of second law efficiency vs T_{lpg}, T_c.

is represented by the area under a dark green color. This maximum efficiency is achieved at a lower value of T_c and T_{hpg}. Conversely, at a higher condenser temperature and high-pressure generator, a minimum value is obtained i.e. less than 0.145.

Contour Plot of Second Law Efficiency vs T_E, T_C

Figure 8 is the contour plot of second law efficiency for decision variable T_c on the X-axis and T_e on the Y-axis. In this contour plot, the area under the dark green color represents the second law efficiency at the maximum value that is more than 0.17. This maximum efficiency is achieved by taking a lower value of T_c and a higher value of T_e. Conversely, the minimum value is obtained at a higher condenser temperature and lower temperature at T_e which is less than 0.14. The significance of this contour plot is that for a particular evaporator temperature the system efficiency would be higher in the winter season as compared to summer.

Contour Plot of Second Law Efficiency vs T_{LPG}, T_A

Figure 9 is the contour plot for second law efficiency against the decision variable T_a and T_{lpg} on the X-axis and Y-axis respectively. As interpreted from the plot, the second law efficiency is maximum that is more than 0.18 which is shown by the area under dark green color. This maximum efficiency is achieved by taking a lower value of T_a and higher Temperature at LPG. Conversely, the second law efficiency is noted lowest (less than 0.15) at a higher absorber temperature and lower temperature at LPG. It also implies that for a fixed absorber temperature, the second law efficiency decrease as T_{lpg} decrease or at a fixed

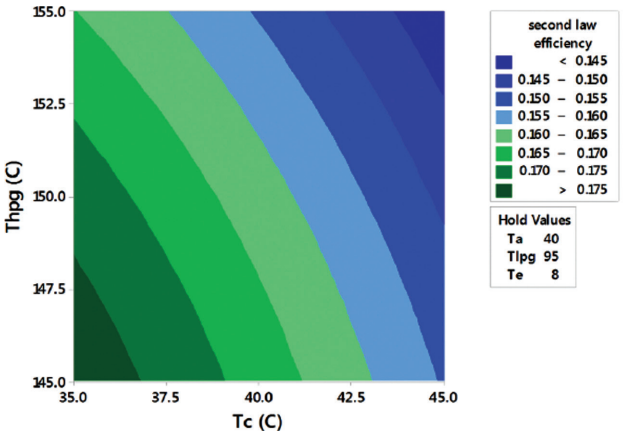

Figure 7. Contour plot of second law efficiency vs T_{hpg}, T_c.

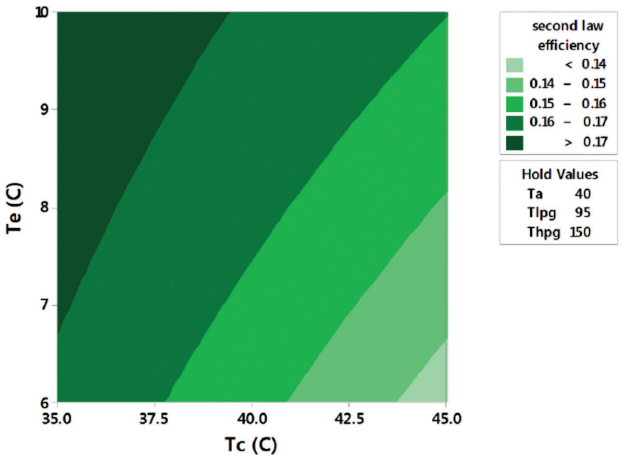

Figure 8. Contour plot of second law efficiency vs T_e, T_c.

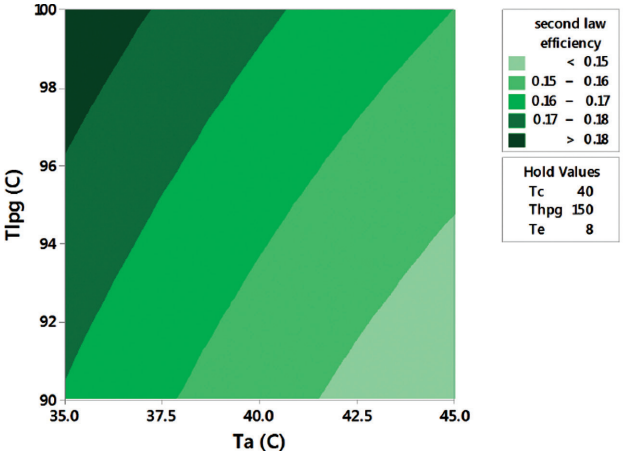

Figure 9. Contour plot of second law efficiency vs T_{lpg}, T_a.

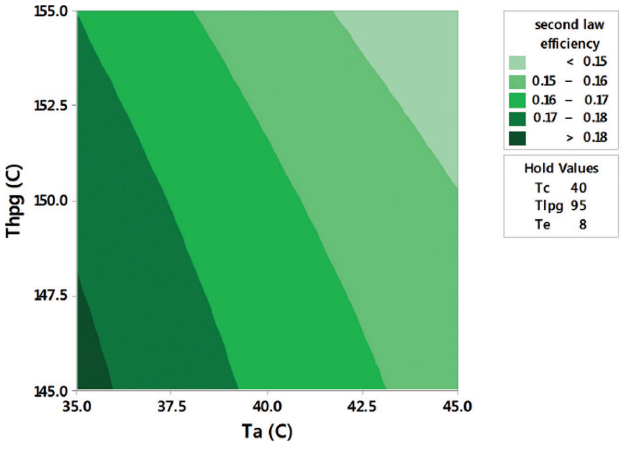

Figure 10. Contour plot of second law efficiency vs T_{hpg}, T_a.

value of T_{lpg}, the second law efficiency would be lower in summer as compared to winter.

Contour Plot of Second Law Efficiency vs T_{HPG}, T_A

Figure 10 is the contour plot of second law efficiency for decision variables T_a and T_{hpg} on the X-axis and Y-axis respectively. In this plot, the area under dark green color depicts second law efficiency with a maximum value that is more than 0.18. This maximum efficiency is achieved by taking a lower value of T_a and T_{hpg}. Conversely, the minimum value is achieved at a higher absorber and high-pressure generator temperature. The minimum value represented is less than 0.15. From the figure, it is worth mentioning that area for maximum second law efficiency is insignificant as compared to other areas, and for absorber temperature greater than 36°C the second law efficiency would be up to 18% irrespective of the temperature of LPG.

Contour Plot of Second Law Efficiency vs T_E, T_A

Figure 11 is the contour plot of second law efficiency for decision variable T_a on the X-axis and T_e on the Y-axis. It is visible in the graph that the second law efficiency is indicated by a peak as represented by the area under dark green color and which is more than 0.18. The area for maximum second law efficiency is quite insignificant. It means practically more than 18 % efficiency is not possible for given values of the decision variable.

Contour Plot of Second Law Efficiency vs T_E, T_{LPG}

Figure 12 is the contour plot of second law efficiency for decision variable T_{lpg} on the X-axis and T_e on the Y-axis. In this contour plot, the area under the dark green color represents the highest value of second law efficiency that is more than 0.170. This maximum efficiency is achieved by taking a higher value of T_e and T_{lpg}. Conversely, the minimum value is obtained at a lower temperature at the evaporator and low-pressure generator. This value is less than 0.145. The iso-efficiency area can be obtained by reducing the temperature at LPG and simultaneously increasing the temperature of evaporator converse is also true.

CSB ANALYSIS

For CSB analysis of a component, the decision variable of the component is varied for a particular range then irreversibility change of that component as well as irreversibility total of the system is computed in that range and then

$$\text{CSB} = \frac{\text{Change in the irreversibility of that particular component}}{\text{Change in irreversibility total of the system}} \quad (4)$$

Table 7. CSB analysis of evaporator

Irreversibility	Te = 6°C	Te = 8°C	Te = 10°C
I_{abs} (kW)	21.05	21.7	22.28
I_{cond} (kW)	4.488	4.482	4.48
I_{evap} (kW)	12.51	10.23	7.981
I_{lpg} (kW)	2.615	3.043	3.493
I_{hpg} (kW)	2.587	2.752	2.931
I_{shx1} (kW)	2.722	2.436	2.194
I_{shx2} (kW)	4.905	4.569	4.29
I_{exp} (kW)	0.7992	0.6852	0.5811

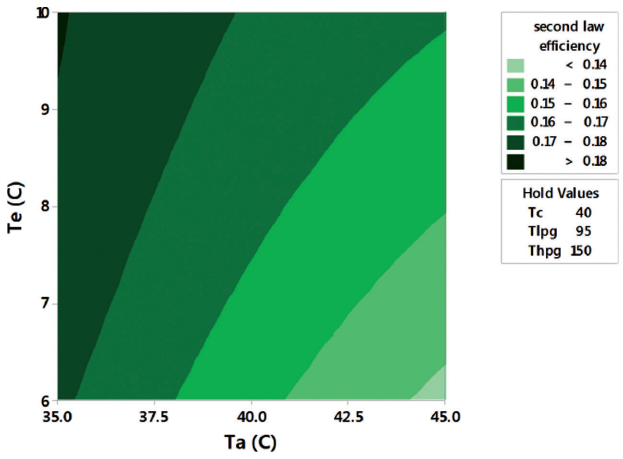

Figure 11. Contour plot of second law efficiency vs T_e, T_a.

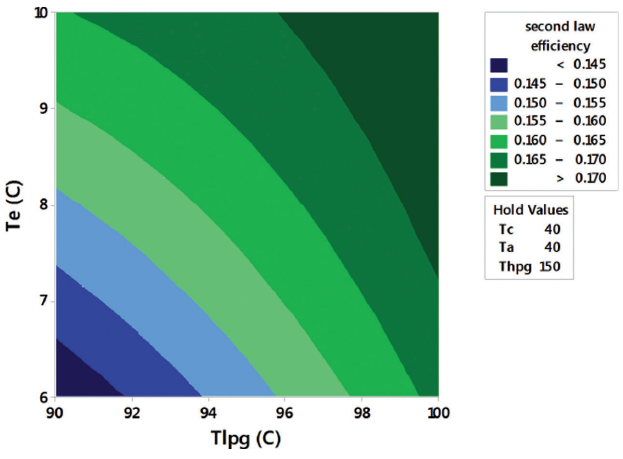

Figure 12. Contour plot of second law efficiency vs T_e, T_{lpg}.

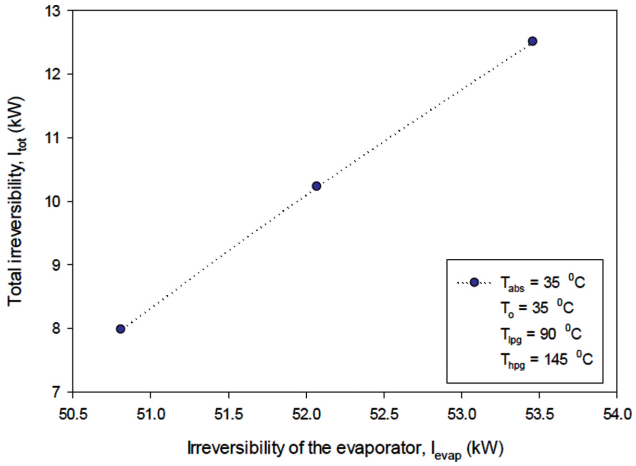

Figure 13. CSB analysis of the evaporator.

In the present analysis CSB analysis of evaporator is conducted. Here three values of evaporator temperature is considered namely T_e = 6°C, T_e = 8°C, T_e = 10°C. The irreversibility of the evaporator, as well as the irreversibility total, is computed for the three mentioned values of the evaporator (refer to Table 7). Figure 13 shows irreversibility total on the Y-axis whereas Irreversibility in the evaporator is shown on the X-axis. Therefore,

$$CSB = \frac{dy}{dx} = 0.5851$$

The CSB < 1 means that the rate of irreversibility change in the evaporator is more than the rate of irreversibility change of the system. It implies that when evaporator temperature has increased the irreversibility in the evaporator decrease but the irreversibility of the other components except for the evaporator increase.

CONCLUSIONS

The present investigation involves RSM-based thermodynamic analysis of VARS which is run by the blowdown heat of a 210 MW thermal power plant situated at Badarpur. The research work yielded significant conclusions which are listed below.

- The Heat recovered during blow-down operation can be used as a source of heat for the vapor absorption refrigeration system. In our study waste heat of blowdown water of 210 MW Thermal Power Station, Badarpur is considered.
- The RSM method is used to identify the decision variable on which second law efficiency does depend. Higher the F value of the decision variable more strongly would affect second law efficiency In our study F value of absorber temperature is = 2049.4, followed by condenser temperature (F value = 1596.4), and is least affected high-pressure generator temperature(F value = 495).This would further help in the design of the experiment.
- In this study, the Iso-second law efficiency curve is plotted against decision variables. The study shows that second law efficiency decrease when Condenser Temperature increase but same value of second law efficiency can be maintained if the temperature of Low-pressure generator increase. Here Condenser Temperature strongly depends upon Coolant temperature which ultimately depends upon ambient temperature thus Condenser temperature is variable so this is the second law of efficiency but this variability can be nullified by altering the temperature of the low-pressure generator.

NOMENCLATURE

T_o	Ambient temperature (K)
HPG	High-pressure generator
Li-Br	Lithium Bromide
$\dot{m}$	Mass flow rate (kg/s)
h	Specific enthalpy (KJ/kg)
C	Specific heat of Li-Br mixture
T	Temperature (K)
COP	Coefficient of Performance
$\dot{Q}$	Heat transfer (KW)
I	Irreversibility (KW)
LPG	Low-pressure generator
X	Mass fraction of Li-Br
s	Specific entropy (KJ/kg-K)
C_{pw}	Specific heat of the water

Greek Symbols

ε_1	Effectiveness of solution heat exchanger 1
η	Efficiency
ε_2	Effectiveness of solution heat exchanger 2

Subscripts

abs	Absorber
e	Evaporator
lpg	Low-pressure generator
c	Condenser
hpg	High-pressure generator
p	Pump

AUTHORSHIP CONTRIBUTIONS

Authors equally contributed to this work.

DATA AVAILABILITY STATEMENT

The authors confirm that the data that supports the findings of this study are available within the article. Raw data that support the finding of this study are available from the corresponding author, upon reasonable request.

CONFLICT OF INTEREST

The author declared no potential conflicts of interest with respect to the research, authorship, and/or publication of this article.

ETHICS

There are no ethical issues with the publication of this manuscript.

REFERENCES

[1] Abed H, Atashkari K, Niazmehr A, Jamali A. Thermodynamic optimization of combined power and refrigeration cycle using binary organic working fluid. Int J Refrig 2013;36:2160–2168. [CrossRef]

[2] Fontalvo A, Pinzon H, Duarte J, Bula A, Quiroga AG, Padilla RV. Exergy analysis of a combined power and cooling cycle. Appl Therm Eng 2013;60:164–171. [CrossRef]

[3] Rêgo AT, Hanriot SM, Oliveira AF, Brito P,. Rêgo TFU. Automotive exhaust gas flow control for an ammonia-water absorption refrigeration system. Appl Therm Eng 2014;64:101–107. [CrossRef]

[4] Parvez M, Khaliq A. Exergy analysis of a syngas fuelled cogeneration cycle for combined production of power and refrigeration. Int J Exergy 2014;14:1–21. [CrossRef]

[5] Goyal R, Sharma D, Soni SL, Gupta PK, Johar D. An experimental investigation of CI engine operated micro-cogeneration system for power and space cooling. Energy Convers Manag 2015;89:63–70.

[6] Yang X, Zhao L, Li H, Yu Z. Theoretical analysis of a combined power and ejector refrigeration cycle using zeotropic mixture. Appl Energy 2015;160:912–919. [CrossRef]

[7] Singh OK. Performance enhancement of combined cycle power plant using inlet air cooling by exhaust heat operated ammonia-water absorption refrigeration system. Appl Energy 2016;180:867–879. [CrossRef]

[8] Talukdar K, Gogoi TK. Exergy analysis of a combined vapor power cycle and boiler flue gas driven double effect water-LiBr absorption refrigeration system. Energy Convers. Manag 2016;108:468–477. [CrossRef]

[9] Sachdeva G, Kumae V, Jain V, Rawat R. Multi-objective optimization of cascade refrigeration system using the concept of modified and advanced exergy, risk level, and thermal inventory. Int J Air-Conditioning Refrig 2020;28:2050036. [CrossRef]

[10] Ifaei P, Rashidi J, Yoo CK. Thermoeconomic and environmental analyses of a low water consumption combined steam power plant and refrigeration chillers – Part 1: Energy and economic modelling and analysis. Energy Convers Manag 2016;123:610–624. [CrossRef]

[11] Guo T, Wang HX, Zhang SJ. Fluids and parameters optimization for a novel cogeneration system driven by low-temperature geothermal sources. Energy 2011;36:2639-2649. [CrossRef]

[12] Goyal A, Sherwani AF, Tiwari D. Optimization of cyclic parameters for ORC system using response surface methodology (RSM). Energy Sources Part A Recover Util Environ Eff 2019;1-14. [CrossRef]

[13] Jain V, Sachdeva G. Energy, exergy, economic (3E) analyses and multi-objective optimization of vapor absorption heat transformer using NSGA-II technique. Energy Convers Manag 2017;148:1096–1113. [CrossRef]

[14] F-chart software, "Engineering Equation Solver, EES," F-Chart Software, Madison, WI, 2012.

[15] Arora CP. Refrigeration and Air Conditioning. 3rd ed. New Delhi: Tata McGraw-Hill Education, 2013. [CrossRef]

[16] Ashwni, Sherwani AF, Tiwari D, Kumar A. Sensitivity analysis and multi-objective optimization of organic Rankine cycle integrated with vapor compression refrigeration system. Energy Sources, Part A Recover Util Environ Eff 2021. https://doi.org/10.1080/15567036.2021.1916132. [Online ahead of print] [CrossRef]

[17] Ashwni, Sherwani AF, and Tiwari D. Exergy, economic and environmental analysis of organic Rankine cycle based vapor compression refrigeration system. Int J Refrig 2021;126:259–271. [CrossRef]

[18] M. Inc., "Minitab 18.1 Statistical Software." State College, USA, 2018.

[19] Kaushik SC, Arora A. Energy and exergy analysis of single effect and series flow double effect water-lithium bromide absorption refrigeration systems. Int J Refrig 2009;32:1247–1258. [CrossRef]